

## **A NOVEL APPROACH FOR RCS REDUCTION USING A COMBINATION OF ARTIFICIAL MAGNETIC CONDUCTORS**

**M. E. de Cos, Y. Álvarez, and F. Las-Heras**

Área de Teoría de la Señal y Comunicaciones  
Departamento de Ingeniería Eléctrica  
Universidad de Oviedo  
Edificio Polivalente, Modulo 8, Campus Universitario de Gijón  
Gijón, Asturias E-33203, Spain

**Abstract**—A thin Artificial Magnetic Conductor (AMC) structure for Radar Cross-Section (RCS) reduction applications is presented. The manufactured prototype, which combines two unit-cell metallization sizes, presenting two resonant frequencies, shows broad AMC operation bandwidth, polarization angle independency, and its angular margin when operating under oblique incidence is also tested. It is shown that significant RCS reduction can be achieved with the proposed AMCs combination even if a  $180^\circ$  phaseshift between reflected waves is not met. Two designs are considered: the already mentioned design combining AMCs with overlapped frequency bands and the second one combining Perfect Electric Conductor (PEC) and AMC surfaces. A comparison between these two designs regarding RCS reduction, supported by measurements in an anechoic chamber, is presented.

### **1. INTRODUCTION**

Radar Cross Section [1–4] reduction has received a lot of attention for many years, being the military applications (stealth technology) among the more attractive ones. The aim is the same in all the scenarios: to reduce the scattered electromagnetic field when illuminating the object-of-interest by an incident wave. There have been three remarkable different solutions proposed for RCS reduction: the use of Radar/Radiation Absorbing Material (RAM), object shaping, and object coating.

RAM materials [5,6], widely used in antenna and RCS measurement facilities in order to avoid echoes in floor and walls, transform the electromagnetic energy into heat, using conductor materials for this purpose. The main drawback of RAMs is their size, which fixes the lower frequency at which an antenna/RCS measurement facility can operate [7].

Another approach when dealing with RCS reduction is object shaping, which aims to reduce the scattered field level in the incoming field direction [8]. This technique is quite complex, and it usually requires a trade-off between operational features and RCS reduction specifications.

The third technique for RCS reduction is based on objects' coating [9, 10], the creation of multiple reflected waves canceling each other as its operational principle.

The fine tuning of the Salisbury screen [11] parameters (a combination of RAM and coating techniques) will result in a zero reflected field [14]. However, this sheet, which consists of a resistive dielectric sheet placed  $\lambda/4$  above a PEC surface, exhibits main drawbacks as its narrow bandwidth and the overall thickness ( $\lambda/4$ ), which limits its practical applications. Improvements in bandwidth and thickness using Frequency Selective Surfaces (FSS) have been recently shown in [12, 13].

The use of simple artificial magnetic surfaces, whose reflection coefficient is  $\rho = +1$ , has been discussed [14–16], highlighting the fact of thickness reduction with respect to the Salisbury screen. Other works [17–19] analyze the effect of coating objects with more complex metamaterials.

An arrangement of PEC (showing  $\rho = -1$ ) and AMC ( $\rho = +1$ ) surfaces in a chessboard-like structure has already been proposed [20–22], with the aim of obtaining two reflected waves with a  $180^\circ$  phase-shift between them. Combination of these reflected waves yields a destructive interference, reducing the scattered field level. The idea presented in [22] is followed in [23], proposing a combination of two AMCs with different resonance frequencies, which yields two operating bands where the RCS of the manufactured surface is below  $-15$  dB [23].

Destructive interferences requires not only a  $180^\circ$ -phaseshift between the waves reflected on the PEC and AMC surfaces, but also the same reflection coefficient amplitude,  $|\rho|_{\text{PEC}} = |\rho|_{\text{AMC}}$ . At this point, it is important to remark the fact that in the case of AMC surfaces, it may happen that  $|\rho|_{\text{AMC}} < 1$ , so PEC-AMC combination may not generate two reflected waves completely canceling each other.

Thus, when combining AMC structures for RCS reduction purposes, if the phase difference between the two combined structures

is  $180^\circ$ , the same reflection coefficient amplitude is needed from both of them in order to obtain two reflected waves that completely cancel each other. If the reflection coefficient amplitude of the two combined structures is similar, even if the phase difference between them does not reach  $180^\circ$ , a larger RCS reduction with respect to the case of having different amplitudes but  $180^\circ$  phase difference can be obtained provided that the AMC operation bands of the two combined AMCs overlap.

The present contribution is based on the same idea as [23, 27], i.e., combining two AMCs with different resonance frequencies, but considering the aforementioned fact related to  $|\rho|$ . In order to obtain the two resonant frequencies (see Fig. 1) the same AMC unit cell design is proposed. The advantage is a simplified design and manufacturing process, jointly with the inner advantages of the selected unit cell [24, 25]. A combination of PEC-AMC surface [21, 22] is also manufactured in order to have a reference result.

## 2. AMC DESIGN

The proposed AMC surface (structure) is based on the unit cell described in [25], designed to work in the 5.8 GHz SHF band. The designed unit cell geometry is shown in Fig. 3. A dielectric substrate, Arlon 25N, with relative dielectric permittivity,  $\epsilon_r = 3.28$ , loss

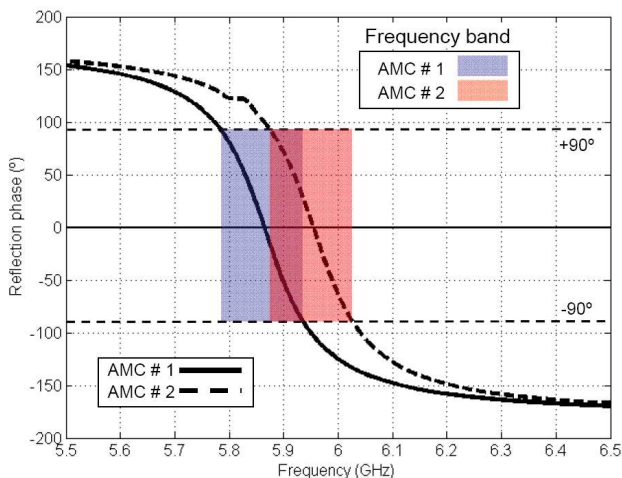


**Figure 1.** Simulated AMC reflection phase vs. frequency. Comparison between AMC designs #1 and #2.

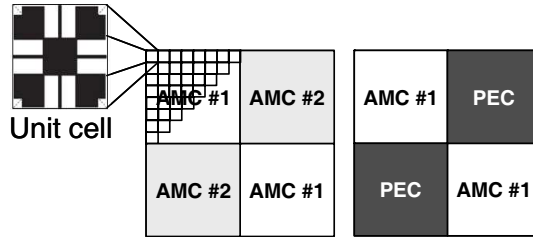


**Figure 2.** Unit cell combination in two different  $2 \times 2$  chessboard-like geometries: AMC #1, 2 and AMC #1-PEC.

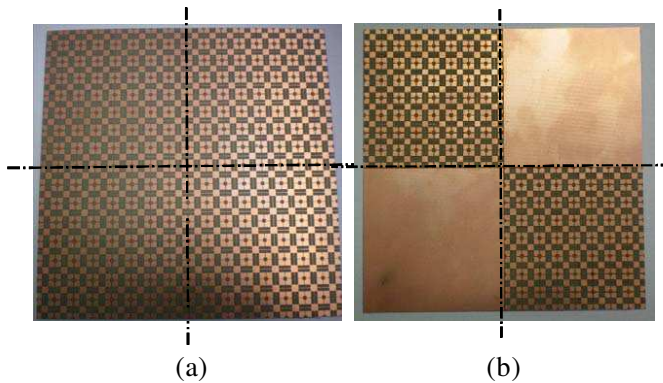


**Figure 3.** Manufactured AMC prototypes (a) AMC #1, 2 and (b) AMC #1-PEC.

tangent less than 0.0025 and a thickness of  $h = 0.762$  mm (30 mils), is used. Unit cell dimensions are  $W \times W = 9.60$  mm  $\times$  9.60 mm, and its geometry exhibits four symmetry planes. The metallization thickness is 18  $\mu$ m. Such dimensions result in the first design (denoted as AMC #1), operating at 5.87 GHz (see Fig. 1), and the AMC frequency bandwidth is approximately 150 MHz (2.5%) [25]. Neither via holes [26] nor multilayer substrates are required, simplifying its practical implementation, its integration with objects (planar microwave devices), and reducing its cost. Other advantages that can be highlighted are low dielectric losses, planar feature and low profile ( $\lambda/67$ ).

The metallization of this unit cell (AMC #1) has been scaled (by reducing its size in a 1% or a 0.01 factor) in order to obtain another unit cell with a different resonant frequency (5.96 GHz), which is denoted as AMC #2. As the two unit cells' metallization size is very similar, their AMC frequency band overlaps (see Fig. 1). The phase difference

between AMC #1 and AMC #2 is less than  $180^\circ$ , so the reflected waves in these two AMC surfaces shall not completely cancel each other.

Unit cells are combined in groups of  $8 \times 8$  cells, being again combined in a  $2 \times 2$  chessboard-like geometry (see Fig. 2) denoted as AMC #1, 2. A second design is obtained by replacing the AMC #2 by a PEC surface, so that a  $180^\circ$  phase-shift is achieved when the AMC #1 reflection phase is zero (at around 5.87 GHz).

### 3. RESULTS

Two  $16 \times 16$  cells planar AMC prototypes have been manufactured using laser micromachining: the first one is a combination of prototypes AMC #1 and AMC #2 (AMC #1, 2; see Fig. 3(a)), and the second one is a combination of AMC #1 and PEC surface (AMC #1-PEC; see Fig. 3(b)). Then the manufactured AMC prototypes have been measured.

At this point, it is important to remark that a frequency shift between simulation and measurement values typically exists. As described in [25] a manufactured prototype of AMC #1 has the resonance at the frequency of  $f = 5.78$  GHz which means a 1.5% deviation with respect to the simulation (5.87 GHz). The cause for this 1.5% shift between the measured AMC resonance frequency and simulated value is typically due to the manufacturing process as justified in [28] and also to the variation of relative dielectric permittivity ( $\epsilon_r$ ) with respect to its nominal value used in the simulations. In the same way, a manufactured prototype of AMC #2 has resonance at the frequency  $f = 5.87$  GHz. So, a frequency shift is expected for the manufactured combined AMC prototypes.

#### 3.1. Measurement Setup in Anechoic Chamber

The manufactured AMC prototype has been tested in a measurement facility. The spherical range in anechoic chamber of the “AntEM-Lab-Universidad de Oviedo” has been adapted to allow RCS measurements. The proposed measurement setup is shown in Fig. 4.

The object-under-test is placed in a roll-over-azimuth positioner, covered by flat laminate RAM in order to minimize reflections due to the metallic positioner structure. Two horn antenna probes working in the 5–7 GHz band have been chosen as Tx and Rx antennas. The separation between each probe and the object-under-test is  $R_{\text{meas}} = 3$  m.

Taking into account the upper limit of the frequency band (7 GHz,  $\lambda = 4.3$  cm) and object-under-test size ( $D = 15.4$  cm), the far-field

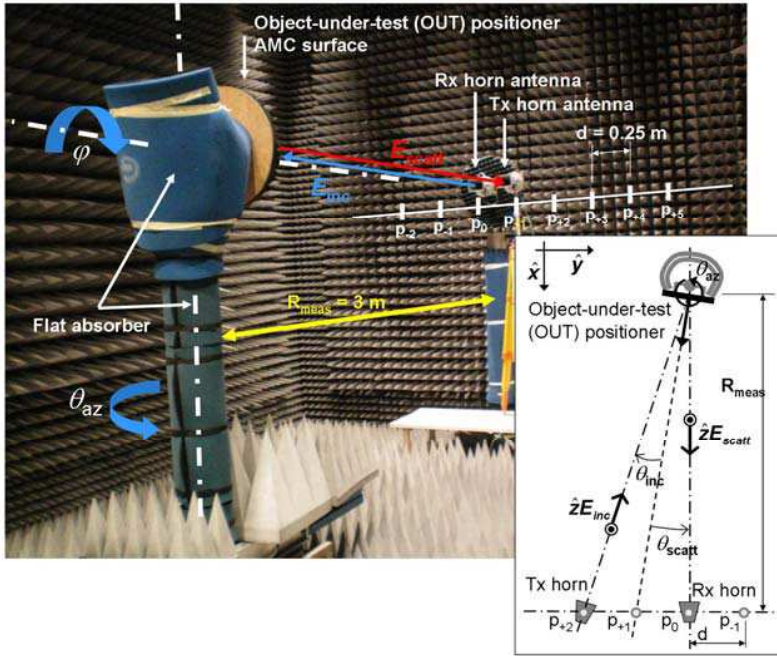


**Figure 4.** RCS measurement setup in anechoic chamber. Different positions for the Tx horn antenna are selected ( $p_n$ ) in order to have different incident ( $\theta_{inc}$ ) and scattering angles ( $\theta_{scatt}$ ).

distance can be estimated as  $R_{FF} = 2D^2/\lambda = 1.1$  m, so the proposed measurement setup ensures that the scattered field is acquired in the far-field region.

In order to test the manufactured AMC prototype for different incidence ( $\theta_{inc}$ ) and scattering ( $\theta_{scatt}$ ) angles, the Tx horn antenna is mounted on a portable tripod, placed at the positions indicated in Fig. 4 as  $p_n$ , being  $n$  from  $-7$  ( $p_{-7}$ ) to  $+7$  ( $p_{+7}$ ) (due to RCS measurement setup mechanical restrictions, it is assumed that  $p_{+n}$  and  $p_{-n}$  are symmetric). The difference between two consecutive positions is  $d = 0.25$  m. The incident ( $\theta_{inc}$ ) and scattering ( $\theta_{scatt}$ ) angles are calculated given the Tx horn antenna position ( $p_n$ ), azimuth angle ( $\theta_{az}$ ) (rotation angle of the object-under-test positioner), and distance  $R_{meas}$  (see the Fig. 4 scheme). Thus, it is possible to evaluate the reflection coefficient amplitude of the AMC structure (which is directly related to the scattered field amplitude) for different scattering angles ( $\theta_{scatt}$ ) vs. incidence angles ( $\theta_{inc}$ ) as depicted in [22]. Finally, the object-

under-test can be rotated in roll ( $\varphi$ -angle), so the RCS response for different field polarization angles can be evaluated.

### 3.2. Quasi-normal Incidence Characterization

First, the AMC frequency response in the operating band is obtained under quasi-normal incidence, placing the Tx horn antenna at the position  $p_{+1}$  and Rx horn antenna at  $p_0$  ( $\theta_{\text{inc}} = \theta_{\text{scatt}} = 2.3^\circ$ ). Fig. 5 represents the reflection coefficient amplitude of the two manufactured prototypes AMC #1, 2, and AMC #1-PEC, compared to the response of a metallic plate (PEC) and the response of AMC #1 prototype presented in [25]. All the manufactured prototypes and metallic plate (“PEC”) have the same size ( $15.36 \text{ cm} \times 15.36 \text{ cm}$ ).

From the measurements plotted in Fig. 5, it can be seen that the AMC #1 reflection coefficient amplitude ( $|\rho|_{\text{AMC \#1}}$ ) is approximately 7 dB lower than the PEC ( $|\rho|_{\text{PEC}}$ ) at  $f = 5.78 \text{ GHz}$  (which is AMC #1 resonance frequency [25]). Thus, the combination of two waves reflected on PEC and AMC #1 surfaces should not cancel completely: the results show that the AMC #1-PEC prototype is unable to reduce the RCS in more than 15 dB.

Last prototype is AMC #1, 2, where the AMC bands are overlapped. According to measurement results, it presents the most

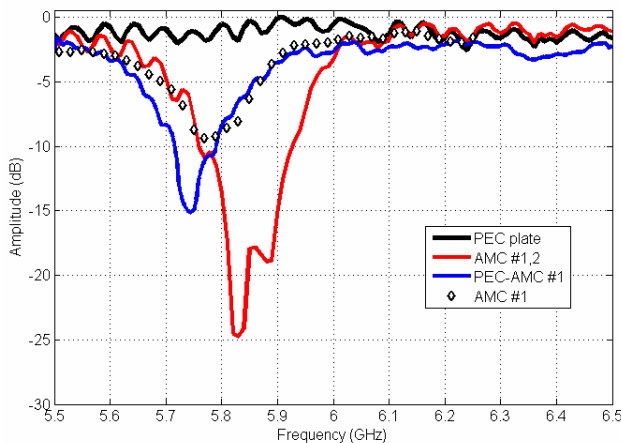


**Figure 5.** Scattered field amplitude for different objects-under-test: the manufactured prototypes AMC #1, 2, AMC #1-PEC, only AMC #1, and the metallic plate (“PEC”). Quasi-normal incidence ( $\theta_{\text{inc}} = \theta_{\text{scatt}} = 2.3^\circ$ ,  $\varphi = 0^\circ$ ).

significant RCS reduction: more than 15 dB in a bandwidth of 95 MHz (1.6% relative to the center frequency). For this design, a  $180^\circ$ -phaseshift is not completely achieved (it is roughly  $130^\circ$ ), but it must be remarked that due to the overlapped frequency bands,  $|\rho|_{\text{AMC}\#1}$  is similar to  $\rho_{\text{AMC}\#2}$  (differences are less than 3 dB), so the reflected waves are interfered destructively.

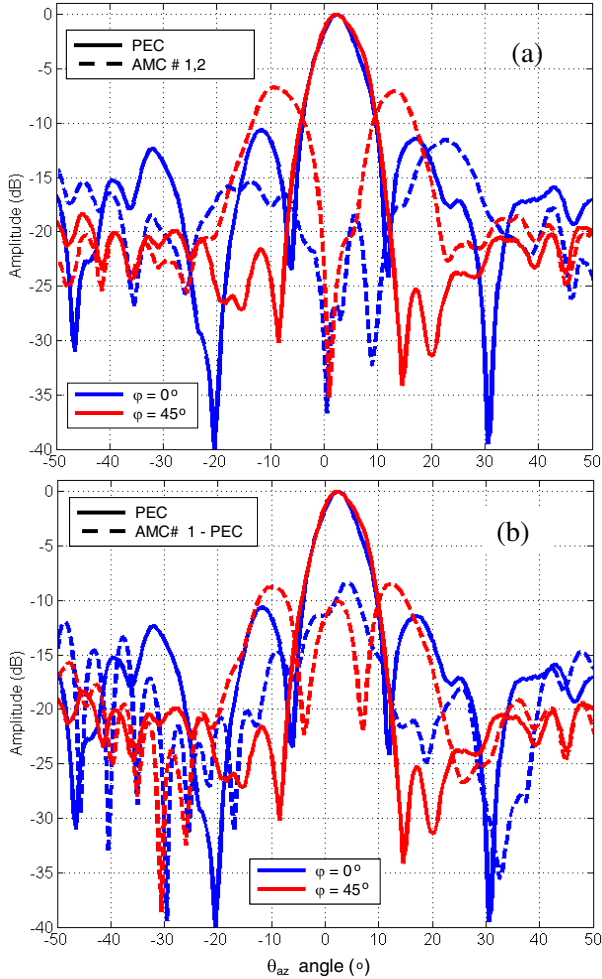
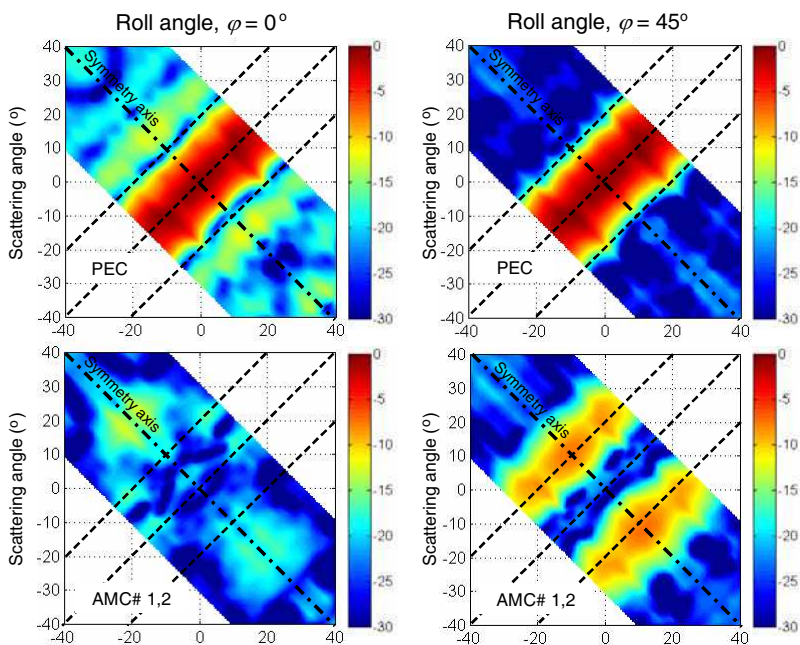


**Figure 6.** Normalized scattered field amplitude as a function of the  $\theta_{az}$ . (a) AMC #1, 2 (frequency,  $f = 5.83$  GHz). (b) AMC #1-PEC (frequency,  $f = 5.74$  GHz).

### 3.3. RCS Measurement for Different Azimuth Angles ( $\theta_{az}$ )

RCS reduction effectiveness has been tested for different azimuth angles ( $\theta_{az}$ ), keeping the Tx and Rx horn antennas fixed: the Tx horn antenna is again placed at the position  $p_{+1}$  and the Rx at  $p_0$ . The selected frequency is  $f = 5.83$  for the prototype AMC #1, 2, which is inside the frequency band where the RCS is reduced more than 15 dB (as depicted in Fig. 5). In the case of AMC #1-PEC, the selected frequency is  $f = 5.74$  GHz.

Figure 6(a) compares the normalized scattered field amplitude vs.  $\theta_{az}$  angle, of a metallic plate and the AMC #1, 2 prototype. For  $\varphi = 0^\circ$ , the maximum of the measured metallic plate RCS (in the  $\theta_{az} = [-50^\circ, +50^\circ]$  interval) is about 12 dB higher than the AMC scattered field (for all the  $\theta_{az}$  interval). However, when rotating the metallic plate and AMC #1, 2 to  $\varphi = 45^\circ$ , the measured AMC #1, 2 scattered field level rises until  $-7$  dB with respect to the maximum of the metallic plate. This is due to constructive interference, depending on the  $\theta_{az}$  angle, AMC prototype electric size, and reflection coefficient of unit cells AMC #1 and AMC #2 [22, 23]. In the case of AMC #1-PEC prototype (Fig. 6) the scattered field for  $\varphi = 45^\circ$  and  $\theta_{az} = 0^\circ$  presents a beam whose level is  $-10$  dB, while the AMC #1, 2 prototype has a null ( $< -35$  dB) at this position.



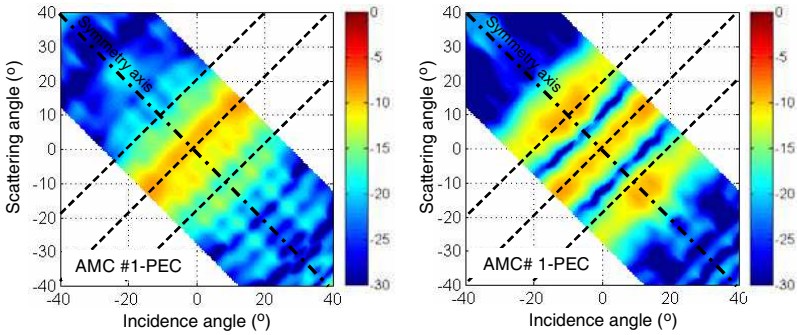


**Figure 7.** Metallic plate scattered field (normalized amplitude, dB) as a function of the incidence angle ( $\theta_{\text{inc}}$ ) and the scattering angle ( $\theta_{\text{scatt}}$ ). Roll angle ( $\varphi$ ) =  $0^\circ$  (left column) and roll angle ( $\varphi$ ) =  $45^\circ$  (right column).

### 3.4. RCS Measurement for Different Incident and Scattering Angles

Next, the field scattered by the metallic plate and AMC prototypes has been evaluated for different incidence and scattering angles. The scattered field amplitude from the metallic plate and from prototypes AMC #1, 2 ( $f = 5.83$  GHz) and AMC #1-PEC ( $f = 5.74$  GHz) is compared in Fig. 7, for a roll angle of  $\varphi = 0^\circ$  (left column) and  $\varphi = 45^\circ$  (right column). For those positions where  $\theta_{\text{inc}} = \theta_{\text{scatt}}$  and  $\varphi = 0^\circ$ , the field scattered by the AMC #1, 2 is more than 20 dB lower than the metallic plate level. In the case of  $\varphi = 45^\circ$ , the scattered field pattern presents two lobes whose normalized level is  $-7$  dB having a null at the position  $\theta_{\text{inc}} = \theta_{\text{scatt}}$ . The other prototype, AMC #1-PEC, presents a higher scattered field level for  $\theta_{\text{inc}} = \theta_{\text{scatt}}$ , that is  $-10$  dB.

In addition, it can be seen the presence of two scattering grating lobes at the angular position of  $\theta_{\text{az}} = +/ - 10^\circ$ . This is due to a constructive interference of the field reflected on the AMC surfaces for these angles. The position of the grating lobes has been studied using the factor array theory in [22].

## 4. CONCLUSION

From the results depicted in Figs. 5–7, it can be concluded that the best RCS reduction performance is achieved with AMC #1, 2 which combines two AMC surfaces with overlapped AMC operation bandwidth, both having similar reflection coefficient amplitude in their frequency bands, although a  $180^\circ$ -phaseshift is not completely

achieved. However, the AMC #1-PEC combination having a  $180^\circ$ -phaseshift reflection coefficient, but different reflection coefficient amplitude, does not ensure a destructive interference in the reflected field yielding a lower RCS reduction.

The interest of the presented AMCs combination relies not only on its significant RCS reduction, but also on the absence of via holes and its low profile, which represent remarkable advantages with respect to previous solutions and make it very attractive due to its simple fabrication and integration, and low cost.

## ACKNOWLEDGMENT

This work has been supported by the “Ministerio de Ciencia e Innovación” of Spain /FEDER” under projects TEC2008-01638/TEC (INVENTA) and CONSOLIDER CSD2008-00068 (TERASENSE), by the “Cátedra Telefónica- Universidad de Oviedo” , by PCTI Asturias under project, PEST08-02 (MATID) and by the Principado de Asturias/FEDER Project IB09-081 (CAMSILOC).

## REFERENCES

1. Lee, K.-C., C.-W. Huang, and M.-C. Fang, “Radar target recognition by projected features of frequency-diversity RCS,” *Progress In Electromagnetics Research*, Vol. 81, 121–133, 2008.
2. Li, N.-J., C.-F. Hu, L.-X. Zhang, and J.-D. Xu, “Overview of RCS extrapolation techniques to aircraft targets,” *Progress In Electromagnetics Research B*, Vol. 9, 249–262, 2008.
3. Pouliguen, P., R. Hémon, C. Bourlier, J.-F. Damiens, and J. Saillard, “Analytical formulae for radar cross section of flat plates in near field and normal incidence,” *Progress In Electromagnetics Research B*, Vol. 9, 263–279, 2008.
4. Alexopoulos, A., “Effect of atmospheric propagation in RCS predictions,” *Progress In Electromagnetics Research*, Vol. 101, 277–290, 2010.
5. Abdelaziz, A. A., “Improving the performance of an antenna array by using radar absorbing cover,” *Progress In Electromagnetics Research Letters*, Vol. 1, 129–138, 2008.
6. Hebeish, A. A., M. A. Elgamel, R. A. Abdelhady, and A. A. Abdelaziz, “Factors affecting the performance of the radar absorbant textile materials of different types and structus,” *Progress In Electromagnetics Research B*, Vol. 3, 219–226, 2008.

7. Hemming, L. H., *Electromagnetic Anechoic Chambers: A Fundamental Design and Specification Guide*, IEEE Press, John Wiley Interscience, 2002.
8. Knott, E. F., J. F. Shaeffer, and M. T. Tuley, *Radar Cross Section*, 2nd edition, 269–276, Artech House, 1993.
9. Oraizi, H. and A. Abdolali, “Combination of MLS, GA & CG for the reduction of RCS of multilayered cylindrical structures composed of dispersive metamaterials,” *Progress In Electromagnetics Research B*, Vol. 3, 227–253, 2008.
10. Chen, H.-Y., P. Zhou, L. Chen, and L. Deng, “Study on the properties of surface waves in coated ram layers and monostatic rcs performances of the coated slab,” *Progress In Electromagnetics Research M*, Vol. 11, 123–135, 2010.
11. Salisbury, W. W., “Absorbent body for electromagnetic waves,” U. S. Patent 2 599 944, Jun. 10, 1952.
12. Kazem, A. Z. and A. Karlsson, “Capacitive circuit method for fast and efficient design of wideband radar absorbers,” *IEEE Trans. on Antennas and Propag.*, Vol. 57, No. 8, 2307–2314, 2009.
13. Abdelaziz, A. A., “A novel technique for improving the performance of salisbury screen,” *Progress In Electromagnetics Research Letters*, Vol. 1, 1–8, 2008.
14. Fante, R. L. and M. T. McCormack, “Reflection properties of the Salisbury screen,” *IEEE Trans. on Antennas and Propag.*, Vol. 36, No. 10, 1443–1454, Oct. 1988.
15. Engheta, N., “Thin absorbing screens using metamaterial surfaces,” *Proc. IEEE Antennas Propag. Societ Int. Symp.*, 392–395, 2002.
16. Zheng, Q.-R., Y.-M. Yan, X.-Y. Cao, and N.-C. Yuan, “High impedance ground plane (HIGP) incorporated with resistance for radar cross section (RCS) reduction of antenna,” *Progress In Electromagnetics Research*, Vol. 84, 307–319, 2008.
17. Zainud-Deen, S. H., A. Z. Botros, and M. S. Ibrahim, “Scattering from bodies coated with metamaterial using FDFD method,” *Progress In Electromagnetics Research B*, Vol. 2, 279–290, 2008.
18. Hady, L. K. and A. A. Kishk, “Electromagnetic scattering from conducting circular cylinder coated by meta-materials and loaded with helical strips under oblique incidence,” *Progress In Electromagnetics Research B*, Vol. 3, 189–206, 2008.
19. Chen, H. T., G.-Q. Zhu, and S.-Y. He, “Using genetic algorithm to reduce the radar cross section of three-dimensional anisotropic impedance object,” *Progress In Electromagnetics Research B*,

- Vol. 9, 231–248, 2008.
20. Zhang, Y., R. Mittra, B. Z. Wang, and N. T. Huang, “AMCs for ultra-thin and broadband RAM design,” *Electronics Letters*, Vol. 45, No. 10, 484–485, 2009.
  21. Zhang, Y., R. Mittra, and B. Z. Wang, “Novel design for low-RCS screens using a combination of Dual-AMC,” *Antennas and Propagation Society Intl. Symposium, 2009. APSURSI'09*, 1–4, Jun. 1–5, 2009.
  22. Paquay, M., J. C. Iriarte, I. Ederra, R. Gonzalo, and P. de Maagt, “Thin AMC structure for radar cross section reduction,” *IEEE Trans. on Antennas and Propag.*, Vol. 55, No. 12, 3630–3638, Dec. 2007.
  23. Iriarte, J. C., et al., “RCS reduction in a chessboard-like structure using AMC cells,” *Proceedings EUCAP 2007*, 1–4, Nov. 11–16, 2007.
  24. Yang, F., K. Ma, Y. Qian, and T. Itoh, “A uniplanar compact photonic-bandgap (UC-EBG) structure and its applications for microwave circuits,” *IEEE Trans. Microwave Theory and Tech.*, Vol. 47, 1509–1514, Aug. 1999.
  25. De Cos, M. E., Y. Álvarez, and F. Las-Heras, “Planar artificial magnetic conductor: Design and characterization setup in the RFID SHF band,” *Journal of Electromagnetic Waves and Applications*. Vol. 23, No. 11–12, 1467–1478, 2009.
  26. Luukkonen, O., C. R. Simovski, and S. A. Tretyakov, “Grounded uniaxial material slabs as magnetic conductors,” *Progress In Electromagnetics Research B*, Vol. 15, 267–283, 2009.
  27. Iriarte, J. C., et al., “Dual band RCS reduction using planar technology by combining AMC structures,” *Proc. Eucap, 2009*, 2009.
  28. Li, Y., et al., “Prototyping dual-band artificial magnetic conductors with laser micromachining,” *Proc. of WARS2006 Conference*, Leura, NSW, Australia, Feb. 2006.